



PART I

INTRODUCTION

1

Basic concepts

1.1 What is a quantum phase transition?

Consider a Hamiltonian, $H(g)$, whose degrees of freedom reside on the sites of a lattice, and which varies as a function of a dimensionless coupling, g . Let us follow the evolution of the ground state energy of $H(g)$ as a function of g . For the case of a finite lattice, this ground state energy will generically be a smooth, analytic function of g . The main possibility of an exception comes from the case when g couples only to a conserved quantity (i.e. $H(g) = H_0 + gH_1$, where H_0 and H_1 commute). This means that H_0 and H_1 can be simultaneously diagonalized and so the eigenfunctions are independent of g even though the eigenvalues vary with g ; then there can be a level-crossing where an excited level becomes the ground state at $g = g_c$ (say), creating a point of nonanalyticity of the ground state energy as a function of g (see Fig. 1.1). The possibilities for an *infinite* lattice are richer. An avoided level-crossing between the ground and an excited state in a finite lattice could become progressively sharper as the lattice size increases, leading to a nonanalyticity at $g = g_c$ in the infinite lattice limit. We shall identify any point of nonanalyticity in the ground state energy of the infinite lattice system as a quantum phase transition: The nonanalyticity could be either the limiting case of an avoided level-crossing or an actual level-crossing. The first kind is more common, but we shall also discuss transitions of the second kind in Chapters 16 and 19. The phase transition is usually accompanied by a qualitative change in the nature of the correlations in the ground state, and describing this change will clearly be one of our major interests.

Actually our focus will be on a limited class of quantum phase transitions – those that are *second order*. Loosely speaking, these are transitions at which the characteristic energy scale of fluctuations above the ground state vanishes as g approaches g_c . Let the energy Δ represent a scale characterizing some significant spectral density of fluctuations at zero temperature (T) for $g \neq g_c$. Thus Δ could be the energy of the lowest excitation above the ground state, if this is nonzero (i.e. there is an energy gap Δ), or if there are excitations at arbitrarily low energies in the infinite lattice limit (i.e. the energy spectrum is *gapless*), Δ is the scale at which there is a qualitative change in the nature of the frequency spectrum from its lowest frequency to its higher frequency behavior. In most cases, we will find that as g approaches g_c , Δ vanishes as

$$\Delta \sim J|g - g_c|^{z\nu}, \quad (1.1)$$

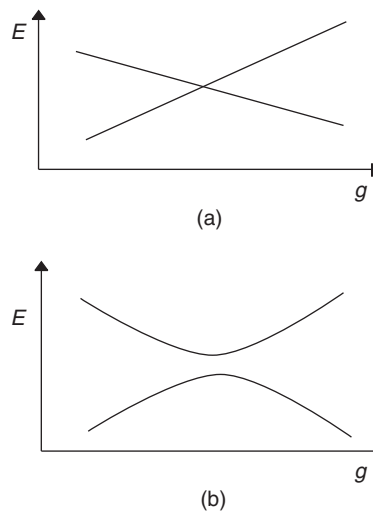


Fig. 1.1

Low eigenvalues, E , of a Hamiltonian $H(g)$ on a finite lattice, as a function of some dimensionless coupling, g . For the case where $H(g) = H_0 + gH_1$, where H_0 and H_1 commute and are independent of g , there can be an actual level-crossing, as in (a). More generally, however, there is an “avoided level-crossing,” as in (b).

(exceptions to this behavior appear in Section 20.2.6). Here J is the energy scale of a characteristic microscopic coupling, and $z\nu$ is a *critical exponent*. The value of $z\nu$ is usually *universal*, that is, it is independent of most of the microscopic details of the Hamiltonian $H(g)$ (we shall have much more to say about the concept of universality below, and in the following chapters). The behavior (1.1) holds both for $g > g_c$ and for $g < g_c$ with the same value of the exponent $z\nu$, but with different nonuniversal constants of proportionality. We shall sometimes use the symbol Δ_+ (Δ_-) to represent the characteristic energy scale for $g > g_c$ ($g < g_c$).

In addition to a vanishing energy scale, second-order quantum phase transitions invariably have a diverging characteristic length scale ξ . This could be the length scale determining the exponential decay of equal-time correlations in the ground state or the length scale at which some characteristic crossover occurs to the correlations at the longest distances. This length diverges as

$$\xi^{-1} \sim \Lambda |g - g_c|^\nu, \quad (1.2)$$

where ν is a critical exponent, and Λ is an inverse length scale (a “momentum cutoff”) of order the inverse lattice spacing. The ratio of the exponents in (1.1) and (1.2) is z , the dynamic critical exponent. The characteristic energy scale vanishes as the z th power of the characteristic inverse length scale

$$\Delta \sim \xi^{-z}. \quad (1.3)$$

It is important to note that the discussion above refers to singularities in the *ground state* of the system. So strictly speaking, quantum phase transitions occur only at zero temperature, $T = 0$. Because all experiments are necessarily at some nonzero, though

possibly very small, temperature, a central task of the theory of quantum phase transitions is to describe the consequences of this $T = 0$ singularity on physical properties at $T > 0$. It turns out that working outward from the quantum critical point at $g = g_c$ and $T = 0$ is a powerful way of understanding and describing the thermodynamic and dynamic properties of numerous systems over a broad range of values of $|g - g_c|$ and T . Indeed, it is not even necessary that the system of interest ever have its microscopic couplings reach a value such that $g = g_c$: it can still be very useful to argue that there is a quantum critical point at a physically inaccessible coupling $g = g_c$ and to develop a description in the deviation $|g - g_c|$. It is one of the purposes of this book to describe the physical perspective that such an approach offers, and to contrast it with more conventional expansions about very weak (say $g \rightarrow 0$) or very strong couplings (say $g \rightarrow \infty$).

1.2 Nonzero temperature transitions and crossovers

Let us now discuss some basic aspects of the $T > 0$ phase diagram. First, let us ask only about the presence of phase transitions at nonzero T . With this limited criterion, there are two important possibilities for the $T > 0$ phase diagram of a system near a quantum critical point. These are shown in Fig. 1.2, and we will meet examples of both kinds in this book. In the first, shown in Fig. 1.2a, the thermodynamic singularity is present only at $T = 0$, and all $T > 0$ properties are analytic as a function of g near $g = g_c$. In the second, shown in

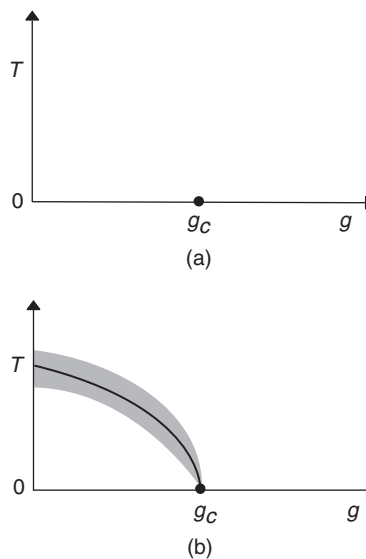


Fig. 1.2

Two possible phase diagrams of a system near a quantum phase transition. In both cases there is a quantum critical point at $g = g_c$ and $T = 0$. In (b), there is a line of $T > 0$ second-order phase transitions terminating at the quantum critical point. The theory of phase transitions in classical systems driven by thermal fluctuations can be applied within the shaded region of (b).

Fig. 1.2b, there is a line of $T > 0$ second-order phase transitions (this is a line at which the thermodynamic free energy is not analytic) that terminates at the $T = 0$ quantum critical point at $g = g_c$.

Moving beyond phase transitions, let us ask some basic questions about the dynamics of the system. A very general way to characterize the dynamics at $T > 0$ is in terms of the thermal equilibration time τ_{eq} . This is the characteristic time in which *local* thermal equilibrium is established after imposition of a weak external perturbation (say, a heat pulse). Here we are excluding equilibration with respect to globally conserved quantities (such as energy or charge) which will take a long time to equilibrate, dependent upon the length scale of the perturbation: hence the emphasis on local equilibration. Global equilibration is described by the equations of hydrodynamics, and we expect such equations to apply in all cases at times much larger than τ_{eq} . We focus here on the value of τ_{eq} as a function of $g - g_c$ and T . From the energy scales discussed in Section 1.1, we can immediately draw an important distinction between two regimes of the phase diagram. We characterized the ground state by the energy Δ in (1.1). At nonzero temperature, we have a second energy scale, $k_B T$. Comparing the values of Δ and $k_B T$, we are immediately led to the important phase diagram in Fig. 1.3. We will see that the two regimes, $\Delta > k_B T$ and $\Delta < k_B T$, are distinguished by different theories of thermal equilibration and of the values of τ_{eq} . In the regime where $\Delta > k_B T$, we will always find long equilibration times which satisfy

$$\tau_{\text{eq}} \gg \frac{\hbar}{k_B T}, \quad \Delta > k_B T. \quad (1.4)$$

One of the important consequences of this large value of τ_{eq} is that the dynamics of the system becomes effectively classical. Thus we can use classical equations of motion to describe the re-equilibration dynamics at the time scale τ_{eq} .

Let us now turn our attention to the important ‘‘Quantum Critical’’ region in Fig. 1.3, where $k_B T > \Delta$. We shall mainly be interested in quantum critical points which are strongly interacting, and not amenable to a nearly-free particle description. In such cases we find a short equilibration time given by

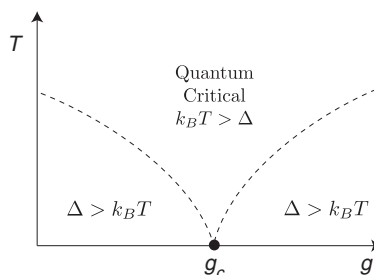


Fig. 1.3

Separation of the phase diagram into distinct regimes determined by the energy scale Δ , which characterizes the ground state, and $k_B T$. The dashed lines are not phase transitions, but smooth crossovers at $T \sim |g - g_c|^{2\nu}$. The phase transition in Fig. 1.2b lies within the $\Delta > k_B T$ region, and is not shown above.

$$\tau_{\text{eq}} \sim \frac{\hbar}{k_B T}, \quad k_B T > \Delta. \quad (1.5)$$

Now the equilibration occurs in a time which is actually independent of the microscopic energy scale J , and is determined by $k_B T$ alone. Moreover, and most interestingly, we cannot use an effectively classical description for the re-equilibration at times of order τ_{eq} . Quantum and thermal fluctuations are equally important in the dynamics in the quantum critical region, and developing a theory for this dynamics will be a central focus of Part III.

What about the $T > 0$ phase transition line in Fig. 1.2b? We have not shown this line in Fig. 1.3. Such a transition should be viewed as reflecting the physics of the $\Delta > k_B T$ region, and so the transition line lies in the corresponding region of Fig. 1.3. In other words, this transition is not really a property of the quantum critical point at $g = g_c$, but of the quantum phase at $g < g_c$. (There could also be a separate transition reflecting the physics of the $g > g_c$ phase, which we have not shown in our phase diagrams.) As we move closer to this phase transition line, we will show that not only does τ_{eq} become long, but so do all the time scales associated with long wavelength thermal fluctuations. Indeed we will find that the typical frequency at which the important long-distance degrees of freedom fluctuate, ω_{typ} , satisfies

$$\hbar\omega_{\text{typ}} \ll k_B T. \quad (1.6)$$

Under these conditions, it will be seen that a purely *classical* description can be applied to these important degrees of freedom – this classical description works in the shaded region of Fig. 1.2b. Consequently, the ultimate critical singularity along the line of $T > 0$ phase transitions in Fig. 1.2b is described by the theory of second-order phase transitions in classical systems. This theory was developed thoroughly in the past three decades and has been explained in many popular reviews and books [59, 172, 244, 312, 557]. We will discuss the needed basic features of this theory in Chapters 3 and 4. Note that the shaded region of classical behavior in Fig. 1.2b lies within the wider window of the phase diagram, with moderate values of $|g - g_c|$ and T , which we asserted above should be described as an expansion about the quantum critical point at $g = g_c$ and $T = 0$. So our study of quantum phase transitions will also apply to the shaded region of Fig. 1.2b, where it will yield information complementary to that available by directly thinking of the $T > 0$ phase transition in terms of purely classical models.

We note that phase transitions in classical models are driven only by thermal fluctuations, as classical systems usually freeze into a fluctuationless ground state at $T = 0$. In contrast, quantum systems have fluctuations driven by the Heisenberg uncertainty principle even in the ground state, and these can drive interesting phase transitions at $T = 0$. The $T > 0$ region in the vicinity of a quantum critical point therefore offers a fascinating interplay of effects driven by quantum and thermal fluctuations; sometimes, as in the shaded region of Fig. 1.2b, we can find some dominant, effective degrees of freedom whose fluctuations are purely classical and thermal, and then the classical theory will apply. However, as already noted, our attention will not be limited to such regions, and we shall be interested in a broader section of the phase diagram.

1.3 Experimental examples

To make the concepts of the previous sections less abstract, let us mention some experimental studies of simple second-order quantum phase transitions. We will meet numerous other examples in this book, but for now we focus on examples directly related to the canonical theoretical models of quantum phase transitions to be discussed in Section 1.4, and in Parts II and III.

- The low-lying magnetic excitations of the insulator LiHoF_4 consist of fluctuations of the Ho ions between two spin states that are aligned parallel and antiparallel to a particular crystalline axis. These states can be represented by a two-state “Ising” spin variable on each Ho ion. At $T = 0$, the magnetic dipolar interactions between the Ho ions cause all the Ising spins to align in the same orientation, and so the ground state is a ferromagnet. Bitko, Rosenbaum, and Aeppli [49] placed this material in a magnetic field transverse to the magnetic axis. Such a field induces quantum tunneling between the two states of each Ho ion, and a sufficiently strong tunneling rate can eventually destroy the long-range magnetic order. Such a quantum phase transition was indeed observed [49], with the ferromagnetic moment vanishing continuously at a quantum critical point. Note that such a transition can, in principle, occur precisely at $T = 0$, when it is driven entirely by quantum fluctuations. We shall call the $T = 0$ state without magnetic order a *quantum paramagnet*. However, we can also destroy the magnetic order at a fixed transverse magnetic field (possibly zero), simply by raising the temperature, enabling the material to undergo a conventional Curie transition to a high-temperature magnetically disordered state. Among the objectives of this book is to provide a description of the intricate crossover between the zero-temperature quantum transition and the finite-temperature transition driven partially by thermal fluctuations; we shall also delineate the important differences between the $T = 0$ quantum paramagnet and the high-temperature “thermal paramagnet;” see Chapters 11, 13, and 14.

A more recent realization of an Ising model in a transverse field has appeared in experiments by Coldea and collaborators [90] on crystals of CoNb_2O_6 , which belongs to the columbite family of minerals. In this case, the Ising spin resides on the Co^{++} ion, again aligned by the spin–orbit interaction to orient parallel or anti-parallel to a crystalline axis. An important difference from LiHoF_4 is that the interactions between the spins are essentially nearest-neighbor, and the long-range dipolar couplings are unimportant; the short-range interactions arise from the Heisenberg exchange process, and their energy scale is determined by the electrostatic Coulomb interactions. Thus CoNb_2O_6 provides a nearly ideal realization of the quantum Ising models which will be the focus of our study in Parts II and III. The dominant exchange couplings are along a particular crystalline axis, and so it is also a useful testing ground for exact results in one dimension.

- Experiments on ultracold atoms in optical lattices by Greiner, Bloch, and collaborators [175] have provided a celebrated example of the superfluid–insulator quantum phase transition. Atoms of ^{87}Rb are cooled to temperatures so low that their quantum statistics

is important. These atoms are bosons and so they ultimately Bose condense into a superfluid state. Then, by applying a periodic potential on the atoms by an optical lattice, Greiner *et al.* localized the atoms in the minima of the periodic potential, leading to a quantum phase transition to an insulating state. At densities where the number of atoms is commensurate with the number of minima of the periodic potential, this transition is described by the $O(2)$ quantum rotor model, which we introduce in Section 1.4 and discuss at length in Parts II and III.

- TiCuCl_3 is an insulator whose only low-lying electronic excitations are rotations of the $S = 1/2$ spins residing on the Cu^{++} ions. Unlike the case for the Co^{++} ions in CoNb_2O_6 , the spin-orbit interactions are relatively weak on Cu^{++} , and a single spin can freely orient along any direction in spin space. A special feature of the crystal structure of TiCuCl_3 is that the Cu atoms are naturally dimerized, i.e. each Cu site has a single partner Cu site, and the exchange interactions are strongest between the partners in each pair. The exchange interaction has an antiferromagnetic sign, and consequently neighboring spins prefer to be oriented in anti-parallel directions. Under ambient pressure, each Cu spin forms a singlet valence bond with its partner, much like that between the two electrons in a hydrogen molecule. Thus although the neighboring spins within a dimer are always anti-parallel, they fluctuate along all directions in spin space in a rotationally invariant manner. We will refer to this state as a quantum paramagnet; it has an energy gap to all excitations above the ground state. Under applied pressure, TiCuCl_3 undergoes a quantum phase transition [414] to an ordered antiferromagnet: a Néel state. In this Néel state, the spins freeze into a definite orientation so that nearby spins are anti-parallel to each other. Such an arrangement is more nearly optimal when the exchange couplings between spins in different dimers are significant. As we discuss below in Section 1.4, this transition between the quantum paramagnet and the Néel state is described by the $O(3)$ quantum rotor model, which will also be discussed in Parts II and III.

1.4 Theoretical models

Our strategy in this book will be to thoroughly analyze the physical properties of quantum phase transitions in two simple theoretical model systems in Parts II and III: the quantum Ising and rotor models. Fortunately, these simple models also have direct experimental realizations in the systems already surveyed in Section 1.3. Below, we introduce the quantum Ising and rotor models in turn, discussing the nature of the quantum phase transitions in them, and relating them to the experimental systems above. Other experimental connections will be discussed in subsequent chapters.

Part IV will survey some important quantum phase transitions in other models of physical interest. Our motivation in dividing the discussion in this manner is mainly pedagogical: the quantum transitions of the Ising/rotor models have an essential simplicity, but their behavior is rich enough to display most of the basic phenomena we wish to explore. It will therefore pay to meet the central physical ideas in this simple context first.

1.4.1 Quantum Ising model

We begin by writing down the Hamiltonian of the quantum Ising model. It is

$$H_I = -Jg \sum_i \hat{\sigma}_i^x - J \sum_{\langle ij \rangle} \hat{\sigma}_i^z \hat{\sigma}_j^z. \quad (1.7)$$

As in the general notation introduced above, $J > 0$ is an exchange constant, which sets the microscopic energy scale, and $g > 0$ is a dimensionless coupling, which will be used to tune H_I across a quantum phase transition. The quantum degrees of freedom are represented by operators $\hat{\sigma}_i^{z,x}$, which reside on the sites, i , of a hypercubic lattice in d dimensions; the sum $\langle ij \rangle$ is over pairs of nearest-neighbor sites i, j . The $\hat{\sigma}_i^{x,z}$ are the familiar Pauli matrices; the matrices on different sites i act on different spin states, and so matrices with $i \neq j$ commute with each other. In the basis where the $\hat{\sigma}_i^z$ are diagonal, these matrices have the well-known form

$$\hat{\sigma}^z = \begin{pmatrix} 1 & 0 \\ 0 & -1 \end{pmatrix}, \quad \hat{\sigma}^y = \begin{pmatrix} 0 & -i \\ i & 0 \end{pmatrix}, \quad \hat{\sigma}^x = \begin{pmatrix} 0 & 1 \\ 1 & 0 \end{pmatrix}, \quad (1.8)$$

on each site i . We will denote the eigenvalues of $\hat{\sigma}_i^z$ simply by σ_i^z , and so σ_i^z takes the values ± 1 . We identify the two states with eigenvalues $\sigma_i^z = +1, -1$ as the two possible orientations of an ‘‘Ising spin,’’ which can be oriented up or down in $|\uparrow\rangle_i, |\downarrow\rangle_i$. Consequently at $g = 0$, when H_I involves only the $\hat{\sigma}_i^z$, H_I will be diagonal in the basis of eigenvalues of $\hat{\sigma}_i^z$, and it reduces simply to the familiar classical Ising model. However, the $\hat{\sigma}_i^x$ are off-diagonal in the basis of these states, and therefore they induce quantum-mechanical tunneling events that flip the orientation of the Ising spin on a site. The physical significance of the two terms in H_I should be clear in the context of our earlier discussion in Section 1.3 for LiHoF_4 and CoNb_2O_6 . The term proportional to J is the magnetic interaction between the spins, which prefers their global ferromagnetic alignment. While the interaction in LiHoF_4 has a long-range dipolar nature, that in CoNb_2O_6 has a nearest-neighbor form like that in (1.7). The term proportional to Jg is the applied external transverse magnetic field, which disrupts the magnetic order.

Let us make these qualitative considerations somewhat more precise. The ground state of H_I can depend only upon the value of the dimensionless coupling g , and so it pays to consider the two opposing limits $g \gg 1$ and $g \ll 1$.

First consider $g \gg 1$. In this case the first term in (1.7) dominates, and, to leading order in $1/g$, the ground state is simply

$$|0\rangle = \prod_i |\rightarrow\rangle_i, \quad (1.9)$$

where

$$\begin{aligned} |\rightarrow\rangle_i &= (|\uparrow\rangle_i + |\downarrow\rangle_i)/\sqrt{2}, \\ |\leftarrow\rangle_i &= (|\uparrow\rangle_i - |\downarrow\rangle_i)/\sqrt{2}, \end{aligned} \quad (1.10)$$

are the two eigenstates of $\hat{\sigma}_i^x$ with eigenvalues ± 1 . The values of σ_i^z on different sites are totally uncorrelated in the state (1.9), and so $\langle 0 | \hat{\sigma}_i^z \hat{\sigma}_j^z | 0 \rangle = \delta_{ij}$. Perturbative corrections in